NANO LETTERS

Letter

pubs.acs.org/NanoLett

A Probabilistic Finite State Logic Machine Realized Experimentally on a Single Dopant Atom

Barbara Fresch,[†,‡] Juanita Bocquel,[§] Sven Rogge,[§] R. D. Levine,[∥,⊥] and F. Remacle*[,†]

[†]Department of Chemistry, B6c, University of Liege, B4000 Liege, Belgium

[‡]Department of Chemical Science, University of Padova, Via Marzolo 1, 35131 Padova, Italy

[§]Centre for Quantum Computation and Communication Technology, School of Physics, The University of New South Wales, Sydney, New South Wales 2052, Australia

[∥]The Fritz Haber Center for Molecular Dynamics and Institute of Chemistry, The Hebrew University of Jerusalem, Jerusalem 91904, Israel

[⊥]Crump Institute for Molecular Imaging and Department of Molecular and Medical Pharmacology, David Geffen School of Medicine and Department of Chemistry and Biochemistry, University of California, Los Angeles, California 90095, United States

Supporting Information

ABSTRACT: Exploiting the potential of nanoscale devices for logic processing requires the implementation of computing functionalities departing from the conventional switching paradigm. We report on the design and the experimental realization of a probabilistic finite state machine in a single phosphorus donor atom placed in a silicon matrix electrically addressed and probed by scanning tunneling spectroscopy (STS). The single atom logic unit simulates the flow of visitors in a maze whose topology is determined by the dynamics of the electronic transport through the states of the dopant. By considering the simplest case of a unique charge state for which three electronic states can be resolved, we demonstrate an efficient solution of the following problem: in a maze of four connected rooms, what is the optimal combination of door opening rates in order to maximize the time that visitors spend in one specific chamber? The implementation takes advantage of the stochastic nature of electron tunneling, while the output remains the macroscopic current whose reading can be realized with standard techniques and does not require single electron sensitivity.

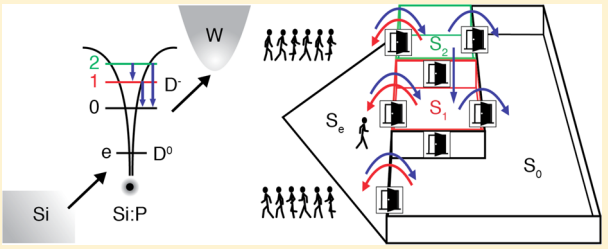

KEYWORDS: *Single electron device, unconventional computing, scanning tunneling spectroscopy, probabilistic logic, finite state machine, single atom transistor*

The increasing ability to experimentally build and manipulate systems at the nanoscale and to exploit quantum effects has a tremendous impact on modern technologies for information processing. Because of high packing density and low-power dissipation, single electron devices (SEDs) are recognized as promising building blocks for innovative logic units.[1−4] As devices approach the size of atoms, quantum phenomena become important, changing the physical model of how information is encoded and processed. To maximize the impact of important technological advances on the fabrication and the control of SEDs, new information-processing principles going beyond the binary switching paradigm of the traditional transistor logic need to be introduced.[5−10]

In recent years, several types of analog and digital circuits have been demonstrated on SEDs by exploiting their specific single-charge transfer characteristics.[4,11] These include multi-valued logic gates,[12,13] complex operations,[14−17] and finite state machines,[18,19] in which the finite response time of the device is used at advantage to store the information to be processed.

One of the major qualitative differences to be considered in scaling down the size of logic devices is the emergence of the inherent randomness that governs the behavior of physical systems at the atomic scale. Randomness is associated with both the variability of nanodevices in terms of structure and properties[20−23] and to the fundamental stochastic nature of quantum processes like electron tunneling.

Within the traditional logic architecture, randomness is mainly associated with noise and errors, thus being considered as a drawback to avoid or to tolerate at best.[24,25] However, different information processing paradigms as the recently proposed approximate computing,[26] noise-based logic,[27,28] but also the more traditional theory of non deterministic automata[29] demonstrate that randomness can represent a resource rather than a drawback, and it can be turned at advantage for the efficient solution of complex logic problems. Therefore, the physical implementation of these principles in

Received: December 12, 2016
Revised: February 7, 2017
Published: February 17, 2017

DOI: 10.1021/acs.nanolett.6b05149
Nano Lett. 2017, 17, 1846−1852

atomic scale devices is a promising avenue to develop innovative architectures for logic processing. The random behavior of single electrons has been used for high-quality random-number generation[30] and stochastic processing for image-pattern matching.[31−33]

A finite state machine (FSM) is an abstract model of computation defined by a set of internal states, its initial state, and the rules governing the transitions among the states. If the rules are given in terms of probabilities, then we are considering a probabilistic FSM.[29,34] In this paper we discuss the design and the laboratory proof-of-concept implementation of a probabilistic finite state machine at the atomic level by harnessing the stochastic nature of the quantum mechanical tunneling of single electrons in and out of a dopant atom in a silicon matrix. The machine is a simulator of the flow through a maze whose topology is dictated by the physical structure of the single electron device. Key ingredients of the device are that the dynamics of electron transfer involves simultaneously several states which are coupled by relaxation processes. The SED consists of a single phosphorus atom embedded in a silicon crystal experimentally probed by low temperature scanning tunneling spectroscopy (STS) at 5K. We demonstrate that the single atom unit provides the solution of a flow optimization problem. Specifically, electron dynamics simulates visitors through a four-chamber maze. We will demonstrate how the single atom machine can solve a specific problem like: *what is the optimal combination of gate opening rates in order to maximize the time that visitors spend in one specific room of the maze?*

Differently from other approaches relying on single-electron manipulation and detection techniques,[38] the output of our logic implementation is deterministic and is given by the reading of the macroscopic tunneling current. This reading can be realized with standard techniques and does not require single electron sensitivity.

Electronic Transport. The sample is fabricated in situ, that is, in the same ultra high vacuum setup as the cryostat containing the STM head. A highly n-doped silicon substrate is annealed, creating a depleted region near the surface as well as a flat surface. This surface is doped with phosphorus atoms (density $\sim 2 \times 10^{11}$ cm^{-2}). The phosphorus doped layer is overgrown epitaxially by 2.5 nm, i.e., ∼18 monolayers, of intrinsic silicon. Finally the reconstructed 2 × 1 (001) Si surface is passivated with hydrogen. This vertical structure allows for resonant single electron transport thanks to the n-doped substrate, which acts as an electron reservoir.[35−37] Due to quantum confinement, several charge and orbital states of the donor system can be resolved by transport measurements on the single atom device.[24,35,36,39] In STS, changing the potential U allows to select the donor states that enter the transport window which is the energy range between the Fermi energy of the n-doped Si substrate and the Fermi energy of the metallic tip. All of the donor states in this window contribute to the tunneling current. An image of the wave function of the electron bound to the P donor is shown in Figure S1A of the Supporting Information (SI) file.

The donor energy levels resolved in the experiment are schematically represented with different colors in the energy diagram in Figure 1A. The one-electron state corresponds to the neutral dopant (D^0) in its ground state, and it is denoted as S_e (in blue). The two-electron states are the ground state S_0 (in black) and two excited states S_1 (in red) and S_2 (in green) of the charged dopant D^-. Electrons tunnel from the Si sample to the tip as pointed out by the arrows with the corresponding

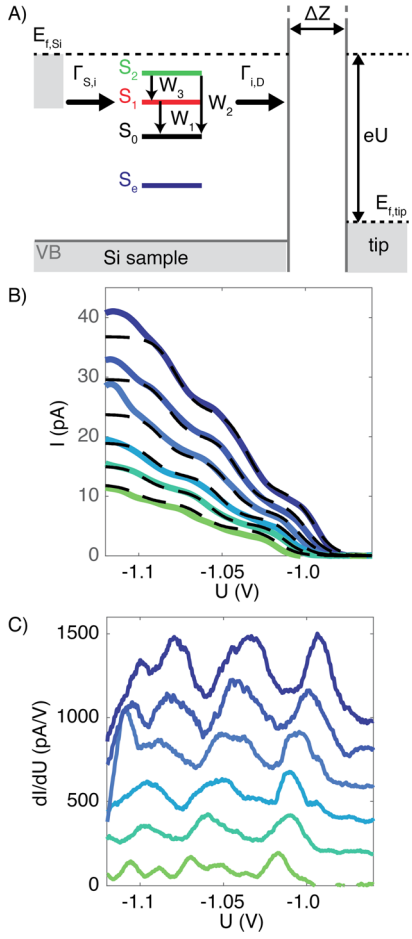

Figure 1. (A) Schematic energy diagram of the single donor energy levels resolved in the STS experiment: the neutral donor D^0 ground state S_e (blue line), the charged donor D^- ground state S_0 (black line), and excited states S_1 and S_2 (red and green lines). U is the applied bias voltage, and ΔZ is the tip−sample distance; VB denotes the valence band in Si, and filled states are shown in gray. The bias window is found between the Fermi energies of the sample $E_{f,Si}$ and the tip $E_{f,W}$. Electrons tunnel from the sample to the tip. (B) Current vs voltage plot corresponding to six values of the tip−sample distance $\Delta Z = Z_0 + Z$, with Z_0 an arbitrary distance and Z varying from 0 to 50 pm with increment of 10 pm. Experimental data (color lines, black: Z = 0 pm, green: Z = 50 pm) and prediction of the kinetic model (dashed black lines). The parameters used to fit the experimental data are given in SI. (C) Corresponding differential conductance dI/dU versus the applied voltage U.

tunneling rates: $\Gamma_{S,i}$ are the tunneling-in rate from the electron reservoir to the i-th energy level of D^-, W_i for i = 1, 2, 3 are intra-atomic relaxation rates between electronic states and $\Gamma_{i,D}$ are the tunneling-out rates from the states of the donor to the tip. Tunneling-in is the fastest process. Depending on the voltage applied to the tip, electrons can tunnel-in (and tunnel-out) to (from) one (S_0), two (S_0 and S_1), or three (S_0, S_1, and S_2) dopant states.

Current−voltage curves show a typical stepwise increase in current when a new state enters the transport window. The height of the steps depends on both tunneling and relaxation processes. Continuous lines in Figure 1B shows the current measured as a function of the applied voltage, U, for six different tip−sample distances $\Delta Z = Z_0 + Z$, with Z_0 an offset distance defined by the feedback parameters (U = −1.45 V and I = 50 pA) and Z varying from 0 to 50 pm with increment of 10

DOI: 10.1021/acs.nanolett.6b05149
Nano Lett. 2017, 17, 1846−1852

pm; panel C shows the corresponding conductance (dI/dU). More details on the experiment can be found in the SI file. The first current step relates to the two-electron (D^-) ground state, S_0, of the dopant, entering the transport window at $U = -1.03$ V. The two following steps correspond to excited states of the two-electron charge state, S_1 and S_2. At short tip−sample distances the conductance plot shows an additional peak at higher energy whose physical origin is difficult to assess and therefore will not be considered further in our analysis.

The current always increases when a new state enters the transport window. Since we are looking at the D^0/D^- transition in a single electron tunneling regime, the next electron can tunnel-in only when the previous one has tunnelled-out. If the electron enters the dopant in an excited state, it can tunnel-out from the same state or it can relax to an electronic state of lower energy. Let us introduce the population vector $\mathbf{P} = [P_0 P_1 P_2 P_e]$ that represents the probability of the possible dopant states. Limiting our attention to the D^0/D^- transition implies $P_e = 1 - P_0 - P_1 - P_2$. The tunneling current can be calculated on the basis of the tunneling-out rates and the populations of the dopant states. A master equation governs the time evolution of the populations, $d\mathbf{P}/dt = \mathbf{K}\cdot\mathbf{P}$, where an element of the kinetic matrix $K_{\alpha\beta}$ is the transition rate from the state α to the state β that depends on the applied voltage and the tip−sample distance through the tunneling rates $\Gamma_{S,i}$ and $\Gamma_{i,D}$ (see eqs 1−3) of the SI for the explicit form of the rates and the kinetic matrix). The measured current is obtained from the stationary solution of the evolution equation, $\mathbf{P}^{st}$, that are the steady-state populations of the dopant at a given bias voltage and tip distance

$$I = e(\Gamma_{0,D}P_0^{st} + \Gamma_{1,D}P_1^{st} + \Gamma_{2,D}P_2^{st}) \quad (1)$$

where e is the elementary charge and the tunneling out rates $\Gamma_{i,D}$ depend on the tip−sample distance (see Figure S3 in the SI). Figure 1B−C reports the calculated current I and conductance dI/dU profiles (dashed lines) that are in excellent agreement with the experimental results (full lines).

By using the master equation, the tunneling of electrons through the dopant is described in terms of a continuous time Markovian dynamics over the discrete set of states $S = \{S_0, S_1, S_2, S_e\}$. This assumption is justified in the regime of weak coupling between the molecule and the electrodes, and it assumes that the waiting times, $T_i = \tau_i - \tau_{i-1}$, between consecutive events are generally large compared to the duration of each charge transfer process. The dynamics is Markovian because the separation of time scales implies that the probability of the system to move to a next state S_{n+1} depends only on the current state S_n and not on the previous dynamical history of the system. If we could follow the microscopic time evolution of the SED starting from the state of a neutral impurity (the D^0 charge state denoted as S_e), we would see an electron jumping at a random time from the source electrode to one of the accessible states of the dopant, for example S_1. Waiting another random time, that electron would either tunnel out to the drain, contributing to the current and leaving the dopant in the S_e state, or relax to the ground state S_0. This *hold-and-jump dynamics* is completely defined by the rate matrix $\mathbf{K}$. The Markov chain implemented by the hold and jump process of electrons through the states of the dopant implements a probabilistic finite state machine.[34,40] The device has several internal states, and it makes transitions between them according to a codified set of probabilities. The state-transition diagram of the single atom machine is drawn in Figure 2A where the states of the machine are defined by the physical states of the dopant (S_0, S_1, S_2, S_e) and their

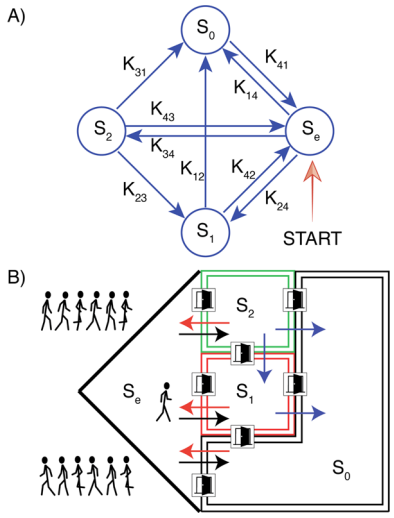

Figure 2. (A) Transition diagram of the probabilistic finite state machine corresponding to the Markov process of the electronic transport. (B) Maze simulated by the probabilistic finite state machine whose transition diagram is reported in panel A.

connections are labeled with the corresponding transition rates. The next reachable states and the probability of transit to each state depend only on the current state of the machine. When the device is in the state S_i, the successor state is chosen with probability $p(S_j|S_i)$

$$p(S_j|S_i) = \begin{cases} \mathbf{K}_{ij}/|\mathbf{K}_{ii}| & \text{if } \mathbf{K}_{ii} \neq 0 \text{ and } j \neq i \\ 0 & \text{if } \mathbf{K}_{ii} \neq 0 \text{ and } j = i \\ 0 & \text{if } \mathbf{K}_{ii} = 0 \text{ and } j \neq i \\ 1 & \text{if } \mathbf{K}_{ii} = 0 \text{ and } j = i \end{cases} \quad (2)$$

The machine is autonomous since it evolves following a set of rules for transitioning between states and producing the output without the need for an input control signal. The network can be mapped on a computational problem; it simulates the flow of visitors in a maze of four chambers connected by gates represented in Figure 2B. The gates are directed, so that gate (i, j) controls the transit from chamber i to j, while flow from j to i is controlled by gate (j, i). Each gate opens independently of all others at random times, and whenever a gate opens anyone waiting to pass will immediately take the opportunity to do so. Over a period $[0, t]$, the gate (i, j) will open at times according to a Poisson process with parameter $\mathbf{K}_{ij}$. Someone moving in this maze, presently waiting in chamber i, will move next to the chamber whose gate from i opens first. The stochastic dynamics associated with the D^0/D^- transition of the SED simulates the motion through the chambers, where a single visitor at a time is admitted into the maze. The stationary populations of the single dopant device represent the long run proportion of time that visitors spent in each chamber. By changing the bias voltage U and the tip−sample distance Z we externally control the opening rates of the gates connecting S_e with S_0, S_1, and S_2 (black and red arrows in Figure 2B), and the stationary populations generated by the device change accordingly. The characteristics of the internal gates (blue arrows in Figure 2) depend on the physics of the

DOI: 10.1021/acs.nanolett.6b05149
Nano Lett. 2017, 17, 1846−1852

specific dopant atom and its interaction with the environment. The microscopic output of the single atom device is generated each time the device makes a transition from the internal states corresponding to D^- (S_0, S_1, S_2) to the neutral state D^0 (S_e) delivering an electron that tunnels to the drain. However, the measurement of a macroscopic current requires a time scale that is longer than the system evolution. Therefore, the macroscopic output of the machine is the experimentally measured tunneling current which depends on the stationary populations of the states according to eq 1.

Relaxation. In the single dopant atom the transport dynamics depends on the competition between the tunneling-out from the excited states and the internal relaxation. This dependence is reflected in the relative amplitude of the current steps and of the conductance peaks measured at different voltages. In Figure 3A the amplitude of the current steps is reported as a function of the tip−sample distance. If the rates of tunneling out from the excited states are much faster than the relaxation rates to the ground state, the peaks at more negative bias are more intense than the peak corresponding to the transport through the ground state only. This condition is realized by setting a short distance between the tip and the sample (small Z). Conversely, if the relaxation to the ground state prevails on the tunneling-out, the conductance peak of the ground state is relatively more intense than the other peaks as is the case at larger distance between the tip and the sample (large Z). The difference in the observed current−voltage profiles is a consequence of the different dynamics underlying the electronic transport, which also determines different stationary populations on the states of the system.

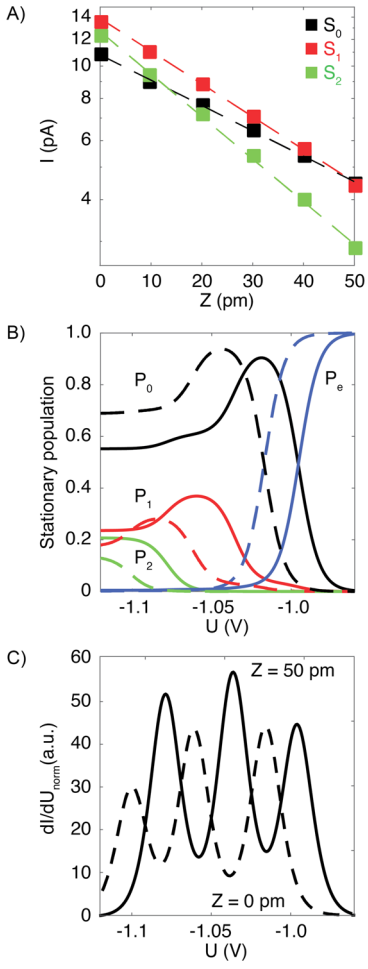

Figure 3. (A) Current step amplitudes as a function of the tip−sample distance variation Z. (B) Stationary populations of S0 (black), S1 (red), S2 (green), and Se (blue) for small (0 pm, solid lines) and large (50 pm, dashed lines) tip−sample distances and (C) the corresponding normalized relative conductance. The parameters of the kinetic model are the same as in Figure 1.

Figures 3B reports the stationary populations $\mathbf{P}^{st} = [P_0^{st} P_1^{st} P_2^{st} P_e^{st}]$ obtained as a long time solution of the kinetic equation as a function of the bias potential for two different sample−tip distances, 0 and 50 pm. At larger tip distances the stationary population of the ground state is increased by the transfer of population from the excited states due to relaxation. In order to compare the current output at different tip−sample distances, we introduce the current scaled by the slowest tunneling rate, I_N, that characterizes the time evolution of the system at a given tip−sample distance

$$I_N = I/(e\Gamma_{0,D}) = P_0^{st} + c_1 P_1^{st} + c_2 P_2^{st} \tag{3}$$

where $c_1 = \Gamma_{1,D}/\Gamma_{0,D}$ and $c_2 = \Gamma_{2,D}/\Gamma_{0,D}$. Once the excited states are within the transport window the rates of tunneling out and their ratios are practically independent of the applied voltage U, we estimate $c_1 = 5$ and $c_2 = 10$ by fitting the experimental data of Figure 1; see SI. The corresponding differential conductance is written as

$$\frac{dI_N}{dU} = \frac{dP_0^{st}}{dU} + c_1 \frac{dP_1^{st}}{dU} + c_2 \frac{dP_2^{st}}{dU} \tag{4}$$

Figure 3C shows the normalized conductance, eq 4, for two different tip−sample distances (0 and 50 pm). For the smaller tip−sample distance (solid line), when the tunneling out is faster than the internal relaxation, the peaks corresponding to the excited states are more intense than the peak of the ground state. For larger tip−sample distance (dashed line) the tunneling out slows down and competes with the relaxation process; consequently the relative intensity of the peaks of the excited states decreases.

The Logic. The different *hold-and-jumps dynamics* of electrons underpinning the measured current at different bias voltage and tip distance correspond, on the logical plane, to different finite state machines. Bearing in mind that each machine simulates the flow through a maze of the type shown in Figure 2B let us formulate the following logic problem:

Given the maze of Figure 2B, assume we can control the rates at which the main gates (black and red doors in Figure 2B) open. However, we ignore the opening rates of the internal doors (blue doors connecting S_0, S_1, S_2). The task is to find the optimal combination of rates for the opening of the main gates in order to maximize the time that visitors spend in chamber 1, independently on the time that visitors spend in the other chambers.

Notice that the solution of this problem requires a significant amount of programming and computing effort with conventional CMOS architectures. One should first analyze the dynamics of visitors in the maze to extract the opening rates of the internal gates and subsequently optimize the rates of the main gates to achieve the target property. However, by using the single atom probabilistic machine, we can implement an alternative and efficient way to find the solution directly at the hardware level.

DOI: 10.1021/acs.nanolett.6b05149
Nano Lett. 2017, 17, 1846−1852

Each single atom device probed at a given bias voltage and tip−sample distance simulates the flow of visitors in the maze for a given set of opening rates. By scanning the bias voltage U and by changing the tip−sample distance Z, we control the relative magnitude of the opening rates of the main gates. Therefore, in an experiment where the transport current is measured as a function of U and Z, we test a family of machines implementing mazes with different opening rates of the main gates. Solving the problem given above amounts to finding the value of the voltage U and of the tip distance Z that maximize the stationary population of the state S_1, the solution will be denoted as (U^*, Z^*). In the following we describe how to achieve this goal by simple manipulations of the experimental measurement.

The procedure is illustrated in Figure 4 with the same model used to reproduce the experimental measurement of Figure 1. Figure 4A and B shows the calculated and experimental 2D maps, respectively, of the normalized differential conductance eq 4 as a function of U and Z. The first step is to identify the three threshold values of voltage corresponding to the entering of a new state in the transport window. These values, that we call U_1, U_2, and U_3 (starting from the less negative), are identified by the three peaks of the differential conductance for each tip−sample distance Z; see also Figure 1C. The maximum of P_1 must be located between U_2 and U_3, in the range of voltage where S_1 is in the transport window and S_2 did not fully enter yet. In order to determine the optimal value $U^*(Z)$ we look for the voltage corresponding to the minimum value of the normalized differential conductance in the domain $[U_2,U_3]$

$$\frac{dI_N}{dU}(U^*) = \min_{[U2,U3]}\left(\frac{dI_N}{dU}\right) = \min_{[U2,U3]}\left(\frac{dP_0^{st}}{dU} + c_1\frac{dP_1^{st}}{dU}\right) \quad (5)$$

The location of the points $U^*(Z)$ that satisfy eq 5 is identified by a white line in Figure 4A. $U^*(Z)$ offers a good estimation of the maximum value of P_1^{st} for each tip−sample distance as long as $c_1 > 1$ (in our model $c_1 = 5$). The next step is to look at the value of the normalized current measured at $U^*(Z)$ as a function of tip−sample distance Z. We then select Z^* by locating the maximum of the current curve, as it is shown in Figure 4C. This simple analysis of the macroscopic output of the experiment gives a good estimation of the control parameters that maximize the stationary population of P_1, meaning that the corresponding tunneling rates are the opening rates that solve the given problem. In other words, the tunneling rates at $(U^*, Z^*) = (-1.058\ \text{V}, 0.8\ \text{pm})$ are the opening rates of the main gates that maximize the time that visitors spend in chamber 1 of the maze, as it is confirmed in Figure 4D. Their numerical values can be extracted on the basis of the dependence of the tunneling rates on the bias voltage and tip distance (as detailed in the SI).

Each single atom device implements a finite state machine whose states and connectivity are compatible with the geometry and transport characteristics of the specific device. Due to the variability of SEDs, each device has its own transport properties. If they are used as switching components in traditional logic units such variability is considered as serious drawback. In our approach, each single atom is a distinct logic unit, so that the same variability becomes richness. In fact, probing another device is equivalent to simulate another set of mazes with different properties. We can then compare their performances establishing which maze keeps the visitor in chamber 1 for a longer time. In Figure 5 we show the

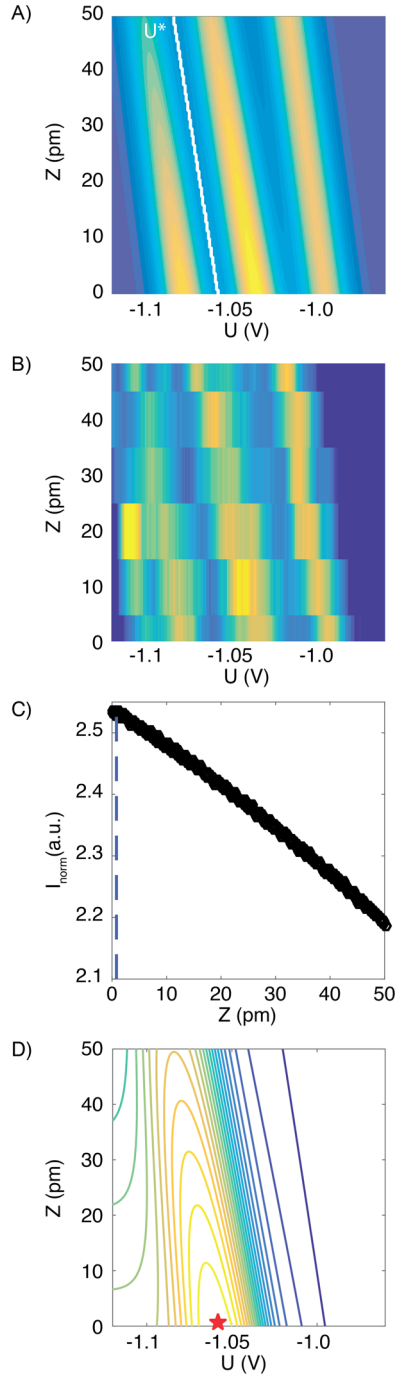

Figure 4. (A) Map of the normalized conductance as a function of the applied potential U and tip distance Z. The white line gives the value of $U^*(Z)$ minimizing the relative conductance in the domain $[U2,U3]$. (B) Experimental map of the normalized conductance for the six values of tip−sample distance investigated in the experiment. (C) Normalized current at the bias voltage $U^*(Z)$ as a function of Z. The maximum defines Z^*. (D) Contour plots of the stationary population of state S1 as a function of the applied potential U and tip distance parameter Z. The red star identifies (U^*, Z^*) representing the solution of the logic problem obtained by applying the procedure discussed in the text. (Color scale: low to high values follows blue to yellow gradient.)

characterization of a device that differs from the experimental model by two aspects: the tunneling barrier is less asymmetric (the ratio of the tunneling-in and the tunneling-out is 4 rather

DOI: 10.1021/acs.nanolett.6b05149
Nano Lett. 2017, 17, 1846−1852

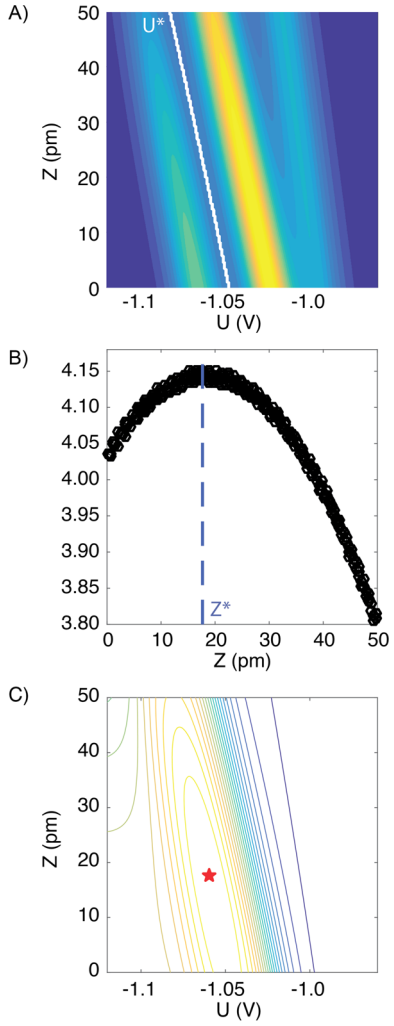

Figure 5. Single atom device for which the tunneling out seed rates $\Gamma_{i,D} = a\Gamma_{S,i} \exp[-bZ]$ are characterized by $a = 1/4$, $b = 90.9$ pm^{-1}, and $\Gamma_{S,1} = 8\Gamma_{S,0}$. The other parameters are the same of the experimental model (see Figure 1). (A) Map of the normalized conductance as a function of the applied potential U and tip distance Z. (B) Normalized current at the bias voltage $U^*(Z)$ as a function of Z. (C) Contour plots of the stationary population of state S1 as a function of the applied potential U and tip distance parameter Z. The red star identifies (U^*, Z^*) representing the solution of the logic problem. (Color scale: low to high values follows blue to yellow gradient.)

than 50), and the tunneling rates of the first excited state are higher (eight times the rates of the ground state rather than five). By performing the same analysis of the macroscopic output we identify the combination (U^*, Z^*) that maximizes the population in chamber 1. As shown in Figure 5B this device produces a normalized current at (U^*, Z^*) that is higher than the current of the device studied in Figure 4. Correspondingly, we also find that the maximum possible population of state 1 is higher (0.43 against 0.37 of the experimental model device). We can then conclude that the maze simulated by this second device outperforms the maze implemented by the experimental model device with respect to the condition specified by the problem at hand.

In summary we demonstrated that the stochastic nature of single electron tunneling in a SED can be used at advantage enabling the physical realization of a probabilistic finite state machine[29,34] used to solve a complex logic problem directly at the hardware level. The number and the connectivity of the internal states of the machine, physically realized by the accessible atomic states, determine the topology of the maze that is simulated. Therefore, progress in precise single atom placement allowing the engineering of "artificial molecules" embedded in a solid state matrix[36,37,41] will open the way to the fabrication of single-molecule logic units capable of simulating and solving networks of increasing complexity. Within our approach, logic functionalities emerge from the physical dynamical response of the device without the need of decomposing neither the problem nor the solution in elementary logic gates. Since the solution of the optimization problem depends on the relative rates of electron transfer and interstate relaxation rate at the hardware level, a wide class of practical problems can be solved in devices for which these parameters can be estimated. Here, we discussed the proof of principle by considering the simplest case of several electronic states of a unique charge state of a single dopant atom within a two-terminal junction. However, the same concepts can be easily applied to systems of complex and customizable topology, including multiple charge states and gated by a third electrode as in a standard transistor geometry. This work suggests that atomic scale devices that exploit stochastic effects to produce low-power and specialized logic units could be an important part of future electronic technology.

■ ASSOCIATED CONTENT

Supporting Information

The Supporting Information is available free of charge on the ACS Publications website at DOI: 10.1021/acs.nanolett.6b05149.

Experimental details of sample preparation and scanning tunneling spectroscopy measurements. Kinetic model for the *hold-and-jump* dynamics of electrons through the dopant (PDF)

■ AUTHOR INFORMATION

Corresponding Author

*E-mail: fremacle@ulg.ac.be.

ORCID

Barbara Fresch: 0000-0002-0988-0644

F. Remacle: 0000-0001-7434-5245

Notes

The authors declare no competing financial interest.

■ ACKNOWLEDGMENTS

This work was supported by the European Commission Future and Emerging Technologies Proactive Project MULTI (317707). B.F. acknowledges the support of the Italian Ministero dell'Istruzione, Università e Ricerca through the grant Rita Levi Montalcini −2013 and F.R. the support of Fonds National de la Recherche Scientifique, FRS-FNRS, Belgium.

■ REFERENCES

(1) Lee, Y.; Lee, S.; Im, H.; Hiramoto, T. *J. Appl. Phys.* **2015**, *117* (6), 064501.

(2) Maeda, K.; Okabayashi, N.; Kano, S.; Takeshita, S.; Tanaka, D.; Sakamoto, M.; Teranishi, T.; Majima, Y. *ACS Nano* **2012**, *6* (3), 2798−2803.

(3) Cervera, J.; Mafé, S. *ChemPhysChem* **2010**, *11* (8), 1654−1658.

DOI: 10.1021/acs.nanolett.6b05149
Nano Lett. 2017, 17, 1846−1852

(4) Mol, J. A.; Verduijn, J.; Levine, R. D.; Remacle, F.; Rogge, S. *Proc. Natl. Acad. Sci. U. S. A.* **2011**, *108* (34), 13969−13972.
(5) Kolmer, M.; Zuzak, R.; Dridi, G.; Godlewski, S.; Joachim, C.; Szymonski, M. *Nanoscale* **2015**, *7* (29), 12325−12330.
(6) Santana Bonilla, A.; Gutierrez, R.; Medrano Sandonas, L.; Nozaki, D.; Bramanti, A. P.; Cuniberti, G. *Phys. Chem. Chem. Phys.* **2014**, *16* (33), 17777−17785.
(7) Carlton, D. B.; Emley, N. C.; Tuchfeld, E.; Bokor, J. *Nano Lett.* **2008**, *8* (12), 4173−4178.
(8) Fresch, B.; Hiluf, D.; Collini, E.; Levine, R. D.; Remacle, F. *Proc. Natl. Acad. Sci. U. S. A.* **2013**, *110* (43), 17183−17188.
(9) Fresch, B.; Cipolloni, M.; Yan, T. M.; Collini, E.; Levine, R. D.; Remacle, F. *J. Phys. Chem. Lett.* **2015**, *6* (9), 1714−1718.
(10) Yan, T. M.; Fresch, B.; Levine, R. D.; Remacle, F. *J. Chem. Phys.* **2015**, *143* (6), 064106.
(11) Lee, S.; Lee, Y.; Song, E. B.; Wang, K. L.; Hiramoto, T. *Appl. Phys. Lett.* **2013**, *102* (8), 083504.
(12) Lee, C. K.; Kim, S. J.; Shin, S. J.; Choi, J. B.; Takahashi, Y. *Appl. Phys. Lett.* **2008**, *92* (9), 093101.
(13) Kim, S.-J.; Lee, C.-K.; Chung, R.-S.; Park, E.-S.; Shin, S.-J.; Choi, J.-B.; Yu, Y.-S.; Kim, N.-S.; Lee, H. G.; Park, K.-H. *IEEE Trans. Electron Devices* **2009**, *56* (5), 1048−1055.
(14) Mol, J. A.; van der Heijden, J.; Verduijn, J.; Klein, M.; Remacle, F.; Rogge, S. *Appl. Phys. Lett.* **2011**, *99* (26), 263109.
(15) Klein, M.; Mol, J. A.; Verduijn, J.; Lansbergen, G. P.; Rogge, S.; Levine, R. D.; Remacle, F. *Appl. Phys. Lett.* **2010**, *96* (4), 043107.
(16) Klymenko, M. V.; Remacle, F. *J. Appl. Phys.* **2014**, *116* (16), 164316.
(17) Kim, S. J.; Lee, J. J.; Kang, H. J.; Choi, J. B.; Yu, Y.-S.; Takahashi, Y.; Hasko, D. G. *Appl. Phys. Lett.* **2012**, *101* (18), 183101.
(18) Yan, Y.; Mol, J. A.; Verduijn, J.; Rogge, S.; Levine, R. D.; Remacle, F. *J. Phys. Chem. C* **2010**, *114* (48), 20380−20386.
(19) Fresch, B.; Verduijn, J.; Mol, J. A.; Rogge, S.; Remacle, F. *EPL* **2012**, *99* (2), 28004.
(20) Cervera, J.; Manzanares, J. A.; Mafe, S. *Nanotechnology* **2011**, *22* (43), 435201.
(21) Cervera, J.; Manzanares, J. A.; Mafe, S. *Nanotechnology* **2009**, *20* (46), 465202.
(22) Fresch, B.; Hanozin, E.; Dufour, F.; Remacle, F. *Eur. Phys. J. D* **2012**, *66* (12), 30575.
(23) Fresch, B.; Boyen, H. G.; Remacle, F. *Nanoscale* **2012**, *4* (14), 4138−4147.
(24) Lansbergen, G. P. *Nat. Nanotechnol.* **2012**, *7* (4), 209−210.
(25) Sadek, A. S.; Nikoli, K.; Forshaw, M. *Nanotechnology* **2004**, *15* (1), 192.
(26) Jie, H.; Orshansky, M. In *Approximate computing: An emerging paradigm for energy-efficient design*; Test Symposium (ETS), 2013 18th IEEE European, May 27−30, 2013; pp 1−6.
(27) Kish, L. B. *Phys. Lett. A* **2009**, *373* (10), 911−918.
(28) Naruse, M.; Aono, M.; Kim, S.-J.; Kawazoe, T.; Nomura, W.; Hori, H.; Hara, M.; Ohtsu, M. *Phys. Rev. B: Condens. Matter Mater. Phys.* **2012**, *86* (12), 125407.
(29) Rabin, M. O. *Information and Control* **1963**, *6* (3), 230−245.
(30) Nishiguchi, K.; Fujiwara, A. *Nanotechnology* **2009**, *20* (17), 175201.
(31) Nishiguchi, K.; Ono, Y.; Fujiwara, A.; Inokawa, H.; Takahashi, Y. *Appl. Phys. Lett.* **2008**, *92* (6), 062105.
(32) Yamanaka, T.; Morie, T.; Nagata, M.; Iwata, A. *Nanotechnology* **2000**, *11* (3), 154.
(33) Westervelt, R. M. *Nature* **2008**, *453* (7192), 166−167.
(34) Booth, T. L. *Sequential Machines and Automata Theory*; John Wiley and Sons, Inc., 1967.
(35) Salfi, J.; Mol, J. A.; Rahman, R.; Klimeck, G.; Simmons, M. Y.; Hollenberg, L. C. L.; Rogge, S. *Nat. Mater.* **2014**, *13* (6), 605−610.
(36) Voisin, B.; Salfi, J.; Bocquel, J.; Rahman, R.; Rogge, S. *J. Phys.: Condens. Matter* **2015**, *27* (15), 154203.
(37) Usman, M.; Bocquel, J.; Salfi, J.; Voisin, B.; Tankasala, A.; Rahman, R.; Simmons, M. Y.; Rogge, S.; Hollenberg, L. C. L. *Nat. Nanotechnol.* **2016**, *11* (9), 763−768.
(38) Ono, Y.; Fujiwara, A.; Nishiguchi, K.; Inokawa, H.; Takahashi, Y. *J. Appl. Phys.* **2005**, *97* (3), 031101.
(39) Dellow, M. W.; Beton, P. H.; Langerak, C. J. G. M.; Foster, T. J.; Main, P. C.; Eaves, L.; Henini, M.; Beaumont, S. P.; Wilkinson, C. D. W. *Phys. Rev. Lett.* **1992**, *68* (11), 1754−1757.
(40) Furia, C. A.; Mandrioli, D.; Morzenti, A.; Rossi, M. *Modeling Time in Computing*; Springer, 2012.
(41) Fuechsle, M.; Miwa, J. A.; Mahapatra, S.; Ryu, H.; Lee, S.; Warschkow, O.; Hollenberg, L. C. L.; Klimeck, G.; Simmons, M. Y. *Nat. Nanotechnol.* **2012**, *7* (4), 242−246.

DOI: 10.1021/acs.nanolett.6b05149
Nano Lett. 2017, 17, 1846−1852